

Supporting Information

Entropy engineering of La-based perovskite for simultaneous photocatalytic CO₂ reduction and biomass oxidation

*Mengchen Wang,^a Liming Li,^{b,c} Yong Li,^d Xuxia Shi,^d Hangxing Ren,^{b,e} Yuetao Sun,^b Kangning Liu,^a Wei Song,^d Huamin Li,^a Haibin Wang,^a Mei Han,^a Xi Wang,^a Christopher Dorma Momo Jr,^a Songhua Chen,^{*f} Lihua Liu,^{*g} Hongyan Liang^{*a}*

^a School of Materials Science and Engineering, Tianjin University, Tianjin 300350, P. R. China.

^b Purification equipment research institute of CSSC, Handan 056027, China.

^c School of Chemical Engineering and Technology, Tianjin University, Tianjin 300072, China.

^d CETC Deqing Huaying Electronics co., LTD.

^e School of Materials Science and Engineering, Shanghai Jiao Tong University, Shanghai 200240, China.

^f College of Chemistry and Material Science, Longyan University, Longyan 364012, China.

^g College of Innovation & Entrepreneurship, Shanghai Jianqiao University, Shanghai, P.R. China.

Corresponding Author

* E-mail: hongyan.liang@tju.edu.cn; songhua@iccas.ac.cn; 13075@gench.edu.cn

Experimental Details

Materials. All the materials are firsthand used without any pretreatment. Iron nitrate nonahydrate ($\text{Fe}(\text{NO}_3)_3 \cdot 9\text{H}_2\text{O}$, 98.5%), Cobalt nitrate hexahydrate ($\text{Co}(\text{NO}_3)_2 \cdot 6\text{H}_2\text{O}$, 99%), Nickel nitrate hexahydrate ($\text{Ni}(\text{NO}_3)_2 \cdot 6\text{H}_2\text{O}$, 98%), Chromium nitrate nonahydrate ($\text{Cr}(\text{NO}_3)_3 \cdot 9\text{H}_2\text{O}$, 99%), Manganese nitrate tetrahydrate ($\text{Mn}(\text{NO}_3)_2 \cdot 4\text{H}_2\text{O}$, AR), Lanthanum nitrate hexahydrate ($\text{La}(\text{NO}_3)_3 \cdot 6\text{H}_2\text{O}$, 99.9%), Citric acid ($\text{C}_6\text{H}_8\text{O}_7$, 99.5%), Absolute ethyl alcohol ($\text{C}_2\text{H}_5\text{OH}$, AR), was purchased from Shanghai Aladdin Co. Ltd. All water was purified by the 18.25 M Ω water filtration system.

Materials Synthesis. The high-entropy perovskite catalysts mentioned in this work were synthesized using sol-gel method and high-temperature calcination method.²¹ In a typical synthesis, $\text{La}(\text{FeCoNiCrMn})\text{O}_3$ (LFCNCM) was fabricated by the steps below. 15 mmol of $\text{La}(\text{NO}_3)_3 \cdot 6\text{H}_2\text{O}$, 3 mmol of $\text{Fe}(\text{NO}_3)_3 \cdot 9\text{H}_2\text{O}$, 3 mmol of $\text{Co}(\text{NO}_3)_2 \cdot 6\text{H}_2\text{O}$, 3 mmol of $\text{Ni}(\text{NO}_3)_2 \cdot 6\text{H}_2\text{O}$, 3 mmol of $\text{Cr}(\text{NO}_3)_3 \cdot 9\text{H}_2\text{O}$ and 3 mmol of $\text{Mn}(\text{NO}_3)_2 \cdot 4\text{H}_2\text{O}$ were dissolved in 40 mL of absolute ethyl alcohol with stirring before adding 30 mmol of citric acid to the solution. After forming a homogeneous solution, the solution was heated at 80 °C with stirring until the liquid evaporated completely. The dried precursor was placed in a porcelain vessel and heated at 1000°C for 3 h in a muffle furnace, with a ramping rate of 10 °C min⁻¹. After cooling to ambient temperature, the product was moved to an agate mortar and ground into powder to attain LFCNCM catalyst. The medium entropy samples $\text{La}(\text{CoNiCrMn})\text{O}_3$ (LCNCM), $\text{La}(\text{FeNiCrMn})\text{O}_3$ (LFNCM), $\text{La}(\text{FeCoCrMn})\text{O}_3$ (LFCCM), $\text{La}(\text{FeCoNiMn})\text{O}_3$ (LFCNM), $\text{La}(\text{FeCoNiCr})\text{O}_3$ (LFCNC) were prepared via the similar steps with corresponding metal source.

Photocatalytic synchronous CO₂ reduction and biomass selective oxidation. The photocatalytic synchronous CO₂ reduction and biomass selective oxidation was performed via Perfectlight PCX 50C multichannel photochemical system. Typically, 5 mg of LFCNCM and 200 mg of xylose were added into a quartz reactor. Then, 20 mL of KOH solution was injected into the above reactor. Before photoreaction, the reactor was degassed with 110 kPa of ultrapure CO₂ (99.9999%) for five times to

build a pure CO₂ atmosphere. Afterwards, the reactor was irradiated under a 10 W LED light resource at 30 °C for 4 h. When the reaction was finished, gas products and liquid products were analyzed by gas chromatography and high-performance liquid chromatography (HPLC), respectively. In the recycling test, the concentration of KOH solution was 0.4 M. The recycled photocatalyst was collected by suction filtration. Then, the collected photocatalyst was washed with deionized water until the filtrate was neutral. Finally, the photocatalyst was dried under 60 °C for 8 h for reuse.

Materials Characterization. Powder X-ray diffraction (XRD) patterns were acquired using a D8 advanced diffractometer with a Cu K α radiation source. The angle range of 2 θ was 20° - 90° with a step of 0.15°. The crystallinity of samples were calculated by JADE, and the lattice plane (1 1 0) was chosen because its highest area ratio among the lattice planes. The scanning electron microscopy (SEM) images were collected by an S4800 cold field emission scanning electron microscope and energy dispersive spectrometer (EDS) under 15 keV accelerating voltage. Microstructure was investigated by JEM-2100F transmission electron microscopy (TEM) with energy dispersive X-ray spectroscopy (EDX) and high-resolution transmission electron microscopy (HRTEM). X-ray photoelectron spectroscopy (XPS) spectrogram which investigates the chemical states of the elements in catalysts was obtained from Axis Supra X-ray photoelectron spectroscopy. The quantitative and qualitative analysis of metallic elements in the sample were conducted by inductively coupled plasma optical emission spectrometry (ICP-OES; Agilent 5110).

Photoelectrochemical measurements. Electrochemical measurements were carried out on a CHI760E electrochemical workstation with a stand three-electrodes system. Among them, a Pt wire was used as the counter electrode, and the reference electrode was the saturated Ag/AgCl. The cleaned F-doped tin oxide glass was used as the working electrode. 5 mg of corresponding photocatalyst and 20 μ L of Nafion (5%) were added into 980 μ L of ethanol to form a homogeneous slurry. The homogeneous slurry was ultrasonicated for 30 min and then coated on the FTO glass. The obtained system was dried at 150 °C for 60 min. The supporting electrolyte was Na₂SO₄ solution (0.5 M) with the pH value of 6.8. The incident visible light source was Xe

lamp (300 W). The photocurrent-time was investigated in the irradiation of Xe lamp at a bias potential of 0.5 V vs. Ag/AgCl. EIS was detected by an AC voltage amplitude of 10 mV at -0.3 V vs. Ag/AgCl over the frequency range from 100,000 Hz to 0.01 Hz. The Mott-Schottky was studied in the electrolyte of Na₂SO₄ (0.5 M), and the frequency of the AC potential was set as 500, 800, and 1000 Hz as well as the amplitude was 10 mV.

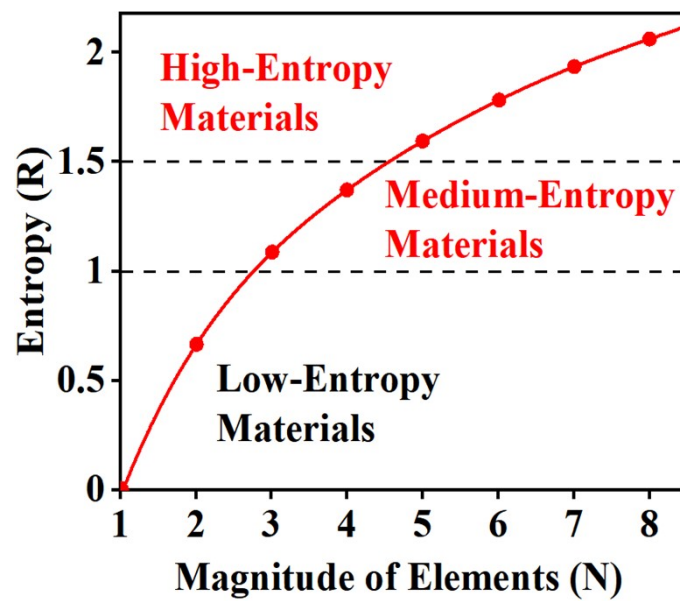


Fig. S1 Relationship between magnitude of elements and configurational entropy.¹

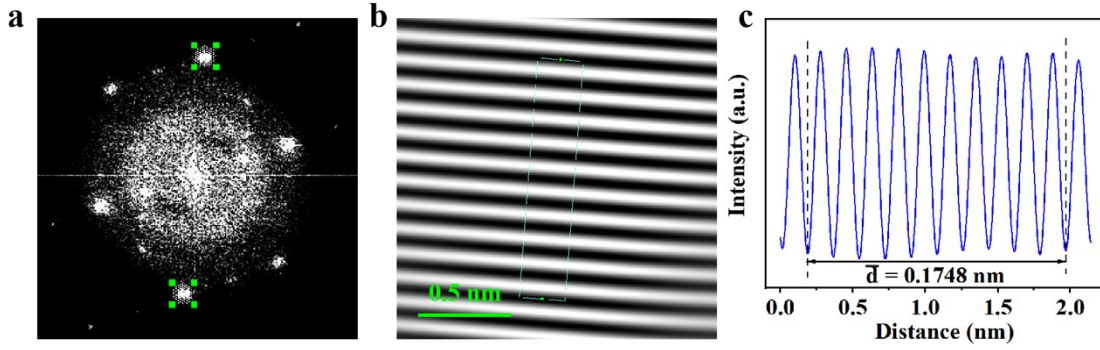


Fig. S2 (a) Fast Fourier Transform (FFT) on the image; (b) Light and dark fringe diagram after inverse FFT; (c) The integrated pixel intensities of (210) planes in LFCNCM.

The indices of crystal facet (hkl) were used to calculate the lattice plane spacings d_{hkl} according to the formula:

$$d = \frac{a}{\sqrt{h^2 + k^2 + l^2}} \quad (1)$$

where a is the lattice constant.

The lattice parameters could be obtained by analyzing HRTEM. Firstly, DigitalMicrograph was used to perform a Fast Fourier Transform (FFT) on the image to obtain diffraction spots (Fig. S2a). A group of symmetric diffraction spots were selected for inverse Fourier transform to obtain the light and dark fringe diagram (Fig. S2b), and the spacing \bar{d} of the fringes (Fig. S2c) was determined and it was calibrated in the HRTEM image (Fig. 1b). An observed interlayer distance of LFCNCM was 0.1748 nm, corresponding well to the lattice plane spacing of the (210) planes shown in the JCPDS 74-1961 (Table S3), which is 0.1739 nm. As a result, the crystal face was determined as (210) planes. According to the HRTEM image, the lattice constant of LFCNCM is calculated by the formula (1) mentioned above, which is 3.9086 Å.

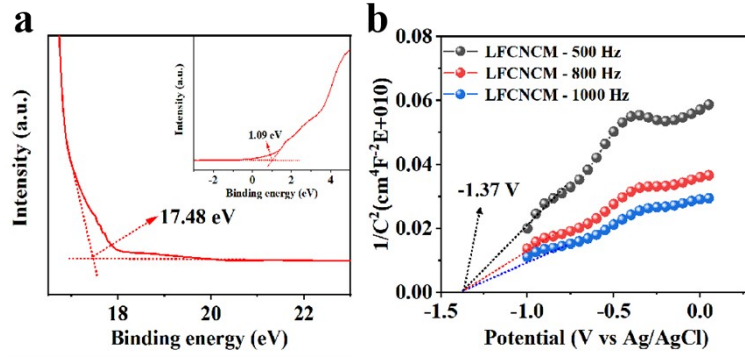


Fig. S3 Band structure of LFCNCM: UPS (a); Mott-Schottky plot (b).

Ultraviolet photoelectron spectroscopy (UPS) is employed to explore the VB and Fermi levels of LFCNCM. From UPS, the VB of LFCNCM can be calculated with the formula^{2, 3}:

$$E_{VB} = 21.20 - E_{cut-off} + E_{SECO} - 4.44 \quad (2)$$

where 21.20 eV is the excitation energy of the applied ultraviolet, and 4.44 eV comes from the energy difference between vacuum level and normal hydrogen electrode (NHE). $E_{cut-off}$ and the energy of the secondary cut-off (E_{SECO}) can be obtained from the intersection at high and low binding energies of UPS (Fig. S3a), respectively. Finally, the VB of LFCNCM is calculated as 0.37 V vs. NHE. To investigate the position of CB, the Mott-Schottky plot of LFCNCM was performed. As depicted in Fig. S3b, the flat band potential (E_{fb}) of LFCNCM is -1.37 V vs Ag/AgCl. Meanwhile, the Mott-Schottky curve of LFCNCM shows a positive slope, suggesting the n-type semiconductor feature for LFCNCM, in which electron serves as the primary charge carrier. For n-type semiconductors, the location of CB is 0.2 V deeper than that of the E_{fb} . Therefore, the CB of LFCNCM is -1.57 V vs Ag/AgCl. For a convenient comparison, the reference electrode should be transformed into NHE with the Nernst formula: $E_{NHE} = E_{Ag/AgCl} + 0.197$ (pH = 7).⁴ Finally, the CB of LFCNCM is calculated as -1.37 V vs NHE. Considering the result of UPS, the band gap of LFCNCM is 1.74 eV.

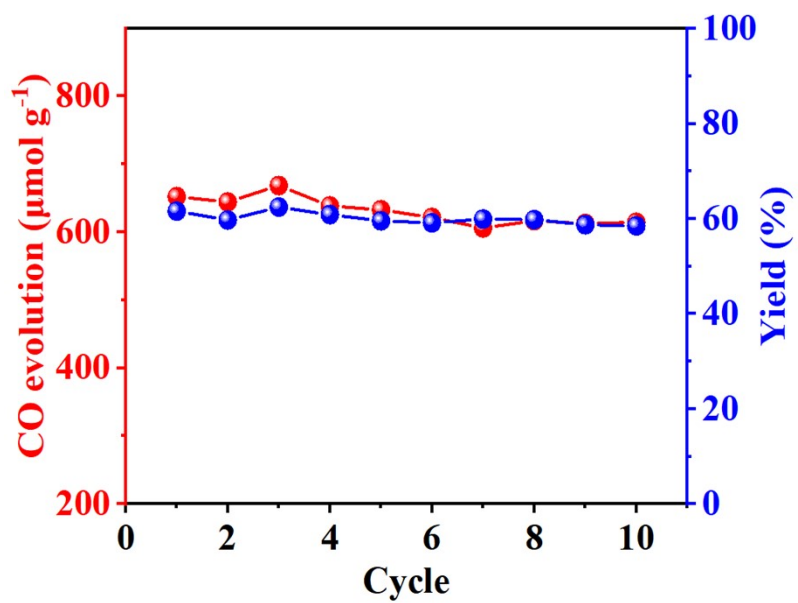


Fig. S4 The recycling test of LFCNCM.

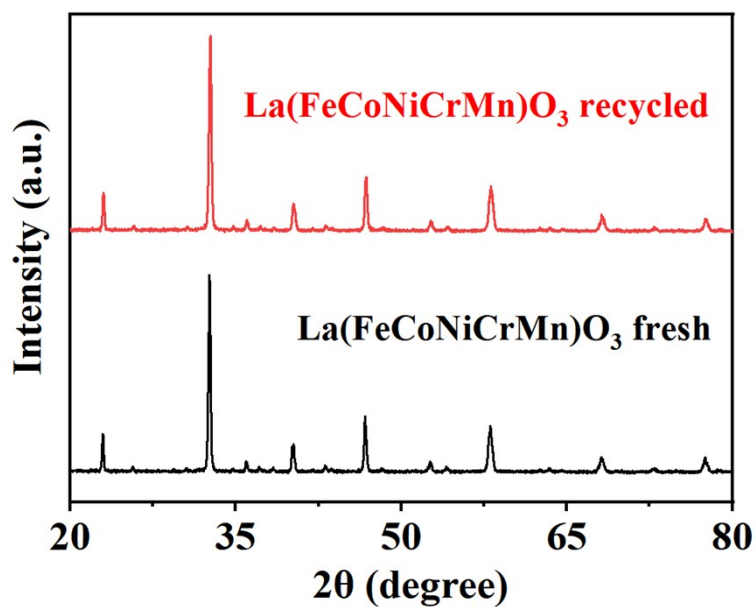


Fig. S5 XRD patterns of LFCNCM before and after 10 cycles operation.

The XRD pattern of recycled catalyst is similar to the fresh, indicating the outstanding structural stability of LFCNCM (Fig. S5).

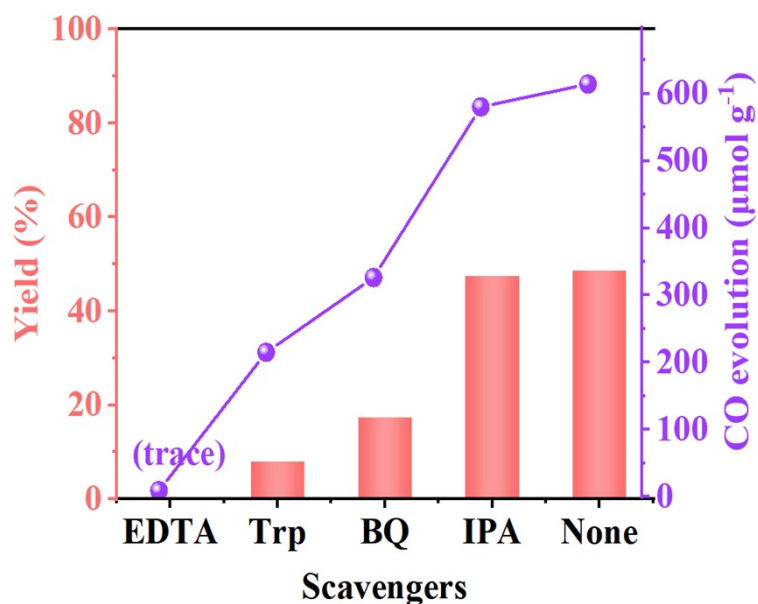


Fig. S6 The effect of various oxidation active species.

To understand the reaction mechanism of biorefinery, the scavenging experiment was performed. 0.5 mmol of various scavengers were added into the reaction system to trap corresponding radicals, in which tryptophan (Trp) for $^1\text{O}_2$, benzoquinone (BQ) for $\cdot\text{O}_2^-$, isopropanol (IPA) for $\cdot\text{OH}$ and ethylenediamine tetraacetic acid (EDTA) for h^+ . As shown in Fig. S6, both xylonic acid yield and CO evolution decreased to the lowest level when EDTA was selected as a scavenger, indicating that h^+ exerted a primary impact on the production of xylonic acid and CO.

Table S1. ICP-OES of LFCNCM.

Elements	Weight composition (%)	Mole ratio (%)
Fe	6.34	11.32
Co	6.44	10.92
Ni	6.44	10.97
Cr	5.91	11.37
Mn	6.24	11.35
La	57.71	41.52

Table S2. The crystallinity results of each sample calculated by XRD.

Sample	Crystallinity (%)
LCNCM	48.67
LFNCM	48.19
LFCCM	55.40
LFCNM	58.09
LFCNC	55.69
LFCNCM	64.15

Table S3. Standard lattice plane spacing and corresponding indices of crystal face from the JCPDS 74-1961.

Lattice Plane Spacing	Indices of crystal face (hkl)
0.3888	(100)
0.2749	(110)
0.2245	(111)
0.1944	(200)
0.1739	(210)
0.1587	(211)
0.1375	(220)
0.1296	(221)
0.1230	(310)
0.1172	(311)
0.1122	(222)

1. A. Sarkar, Q. S. Wang, A. Schiele, M. R. Chellali, S. S. Bhattacharya, D. Wang, T. Brezesinski, H. Hahn, L. Velasco and B. Breitung, *Adv. Mater.*, 2019, **31**, 1806236.
2. S. Bhowmick, C. P. Saini, B. Santra, L. Walczak, A. Semisalova, M. Gupta and A. Kanjilal, *ACS Appl. Nano Mater.*, 2023, **6**, 50-60.
3. Q. Liu, C. C. Chen, K. J. Yuan, C. D. Sewell, Z. G. Zhang, X. M. Fang and Z. Q. Lin, *Nano Energy*, 2020, **77**, 105104.
4. Q. Li, S. C. Wang, Z. X. Sun, Q. J. Tang, Y. Q. Liu, L. Z. Wang, H. Q. Wang and Z. B. Wu, *Nano Res.*, 2019, **12**, 2749-2759.